



3D structured biochip for label free determinations at the point-of-need

G. Zisis^{a,*}, G. Papageorgiou^a, V. Anastasiadis^b, P. Petrou^b, I. Raptis^a, N. Papanikolaou^a

^a Institute of Nanoscience & Nanotechnology, NCSR "Demokritos", Athens 15341, Greece

^b Immunoassays/Immunosensors Lab, Institute of Nuclear & Radiological Sciences & Technology, Energy & Safety, NCSR "Demokritos", Athens 15341, Greece

ABSTRACT

A novel optical label-free biosensing approach is introduced aiming to remove the current limitations of optical biosensors in their application of on-site food analysis. The proposed methodology (GRADual thin film IntErferometry, GRADE) is based on light interferometry employing an illumination source of a few nm spectral width and a 3D micro-patterned sensor surface consisting of multilevel staircase structures, fabricated through grayscale electron beam lithography and appropriate pattern transfer on thick dielectric layer. The formation of the biomolecular adlayer on the 3D structured surface sensor, is monitored with a 2D camera, without the need for broadband illumination sources and spectral analysis instrumentation. Consequently, this novel sensing approach has the potential to enable the cost-efficient monitoring of bioreactions employing a simple optical setup, a low-cost photodetector and light source, thus being an ideal platform for use at the Point-of-Need. In the present study the system is demonstrated for the detection of aflatoxin B₁ (AFB₁), a very potent carcinogen detected in various food categories.

1. Introduction

In the last decades there has been intense research activity in the development of advanced and cost-effective bioanalytical systems based on label-free optical biosensors [1]. Due to their high detection sensitivity, short assay duration and compact size, such systems have a high potential for applications at the Point-of-Need (PoN), thus diminish the need for expensive and time-consuming laboratory analysis.

A variety of different optical sensing principles, such as planar waveguides, plasmons, broad spectrum interferometry and optical fibers have been so far employed to quantitatively determine the concentration of analytes in biological, food or environmental samples [2]. In most of those principles, the biomolecular layer that grows on the sensor's surface during the bioreaction is detected as a shift in the recorded spectrum. Despite the advantages of these sensors, the currently available commercial systems are not suitable for use outside a laboratory. For surface Plasmon Resonance (SPR) and despite its widespread adoption [2], several limitations have been identified such as: the refractive index variation of the liquid medium where the bioreactions take place, a limited number of bioreactions could be monitored simultaneously, and the high cost of the disposable sensor surface [3].

On the other hand, commercial devices based on reflected light spectroscopy (Reflectance Interference Spectroscopy [4–6] or BioLayer Interferometry, [7,8]) are characterized by significant advantages: a relatively simple instrumentation, no need of (or straightforward) optical alignment, and low cost biochips. However, such systems require high-resolution spectrometers which increase significantly the cost of

the final device [9,10]. In addition, the simultaneous determination of more than one analyte in a sample requires the use of motorized set-ups that substantially increase the complexity of the system, the noise of the measurement, and the size and cost of the measurement apparatus thus reducing the possibility for application at the Point-of-Need.

Aiming to small-size low cost biosensing systems, in the past, our group has developed an optical sensing platform based on White Light Reflectance Spectroscopy (WLRS) [11], where the sensor surface is a uniform layer of a silicon dioxide dielectric material on a reflective silicon surface, which under broadband illumination produces characteristic interference fringes across the visible and near infrared spectrum. The growth of the biomolecular layer on the sensor surface due to bioreaction, causes a spectral shift in the reflectance spectrum to higher wavelengths that is monitored in real time by using a dedicated optical probe (6 illumination fibers – 1 collection fiber) and a spectrometer. By employing this principle of operation, several analytes have been quantitatively determined in a wide range of diverse applications including health [12,13], food safety [14,15], and forensics [16]. In addition, by further advancing the WLRS method, the simultaneous determination of two analytes in the same sample has been demonstrated [17], however, the simultaneous determination of more than three analytes is still questionable. This limitation along with the need of a high-resolution spectrometer in the measurement set-up could be proved a hurdle in application at the Point-of-Need.

In the present work, we introduce a radical biosensing approach that is based on thin film interferometry using a sensing area with a gradually-varying-thickness dielectric, aiming to improve the cost

* Corresponding author.

E-mail address: g.zisis@inn.demokritos.gr (G. Zisis).

<https://doi.org/10.1016/j.mne.2022.100117>

Received 25 November 2021; Received in revised form 9 January 2022; Accepted 22 February 2022

Available online 26 February 2022

2590-0072/© 2022 The Authors. Published by Elsevier B.V. This is an open access article under the CC BY license (<http://creativecommons.org/licenses/by/4.0/>).

effectiveness of the system by replacing the spectrometer unit with a CCD or CMOS pixel array and the broadband illumination with a narrow band illumination source. The analytical capabilities of this new label-free approach are demonstrated through the immunochemical determination of Aflatoxin B₁ (AFB₁) which is the most carcinogenic and toxic aflatoxin produced by fungi.

1.1. Theory of sensing principle

Spectral interferometric techniques, monitor and analyze the reflectance interference fringes created upon interaction of light with a planar sensor surface to detect changes in the length of the optical path caused by specific bioreactions occurring between binding molecules immobilized onto the surface and complementary biomolecules in the sample. The proposed optical immunosensor (GRADual thin film Interferometry, GRADE) is based on interferometry of reflected narrow band light from a 3D structured layer of SiO₂ of spatially varying thickness on top of a Si substrate, where the bioreactions take place. Since the transparent SiO₂ layer is not planar but consists of multiple regions with different thickness, the corresponding reflected light intensity of each one of them is different, thus creating an “interference” pattern depending on the designed surface thickness profile that can be recorded from a CCD array.

In the example depicted in Fig. 1a, the thickness of the uniform SiO₂ layer corresponds to one minimum in the 400–700 nm spectral range, which shifts to higher wavelengths due to the bioreaction providing the means for its real time monitoring with the WLRS set-up. By careful design (i.e., by adjusting the thickness range) of the 3D structured SiO₂ film prepared following GRADE methodology, the number of extrema (minima and maxima) displayed in the CCD can be tuned, as shown in Fig. 1b, to obtain a reflectance intensity profile along the surface for monochromatic light, similar with the WLRS spectral interference pattern. When a biomolecular layer built up on top of the dielectric film in both methodologies (WLRS and GRADE), the optical path changes and a shift is detected. However, we should note that, despite the similarity, the two methods have different detection principles. In the WLRS methodology, we measure a spectral shift, while in the GRADE

methodology, reflectance variation is observed by a pixel shift.

2. Materials and methods

For the realization of the 3D structured sensing substrate, a fabrication flow-chart was developed, based on electron beam lithography (EBL), via careful local tuning of the exposure dose, according to the characteristic contrast curve of the resist employed. In order to analyze the reflection signal by as many CCD pixels as possible, grayscale EBL was employed. This technique allowed for tailor-made pattern transfer and fabrication of multiple sensor surfaces, each one designed to assume a 3-dimensional topography on 3- μm thick thermally grown SiO₂ layers on top of Si wafers, with thickness difference between adjacent regions, of the order of 15 nm. The fabrication steps followed, and the first design (linear adjacent regions) of the structured surface are schematically depicted in Fig. 2. Following cleaning in a Piranha solution, dehydration and coating with HMDS (hexamethyl disilazane) to improve resist adhesion, the 4” SiO₂/Si wafers with were spin coated with negative tone resist AR-N 7520.18 (AllResist GmbH) [18] at 1000 rpm and subsequently baked at 85 °C on a hot plate for 65 s. Dose-modulated e-beam exposure was performed using a Raith EBPG 5000+ e-beam writer operating at 100 kV, with a beam current set to 7 nA. Wafers were developed for 120 s by immersion and gentle stirring in 0.16 N TMAH (tetramethylammonium hydroxide) aqueous solution, at room temperature.

For the given process parameters, the exposed resist led to low contrast values (γ), typically equal to 1.14 ± 0.1 . The exposure dose matrix, ranged from 78 to 184C/cm² and was carefully sequenced to exploit the locally non-uniform development rates observed during the development process, in order to achieve an even height step difference, as illustrated in Fig. 2. Subsequently, a thermal reflow step to modify the shape of the “binary” resist structure was performed at 150 °C (T_{reflow} , above the resist’s T_g) for 5 min to smoothen the surface. Following thermal reflow, the resist structure was transferred into the SiO₂ layer using a standard CHF₃ reactive ion etching process at an etch rate of 28 nm min⁻¹ in SiO₂ and 15 nm min⁻¹ in AR-N. After resist stripping, each chip (sensor surface) was diced and prepared for functionalization and encapsulation with a dedicated microfluidic cell. The first design of the 3D structure was a single row of adjacent regions of linearly varied thickness (Fig. 3a), while the final design employed the adjacent regions i on a raster 11×4 arrangement (Fig. 3b), each one with dimensions of 300 $\mu\text{m} \times 400 \mu\text{m}$, covering the entire field of view of the camera.

Thickness measurements at each region exposed at different e-beam dose were performed using a FR-uProbe (ThetaMetrisis) thickness determination system with a measurement spot size of 25 μm . The experimental reflectance spectra acquired in the 450–700 nm wavelength range were fitted based on the theoretical model and the thickness of the photoresist (prior RIE etching) and SiO₂ layer (after RIE etching) were determined at each region. The plot of SiO₂ layer thickness values obtained at each region versus the dose-modulated e-beam exposure conditions used (Fig. 3a) shows a linear trend of the thickness slope, indicating great control of the process. Surface topography examination with an optical profilometer (Fig. 3c) confirmed the designed step height difference between the regions (d).

The optical setup for bioreaction monitoring was based on a

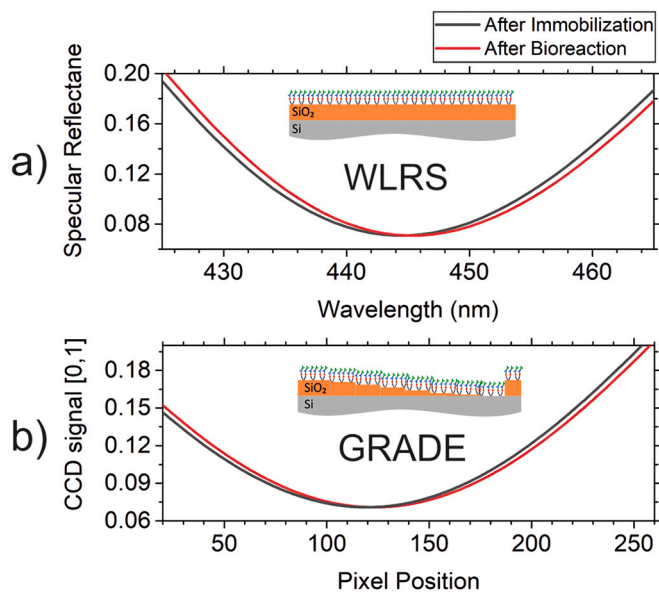


Fig. 1. (a) Reflection spectrum from a chip with fixed SiO₂ thickness (WLRS methodology) and (b) CCD response from a chip with a 3D structured SiO₂ layer (GRADE methodology) upon immobilization of a binding molecule on the sensor surface (black line), and after its bioreaction with a complementary biomolecule (red line). (For interpretation of the references to colour in this figure legend, the reader is referred to the web version of this article.)

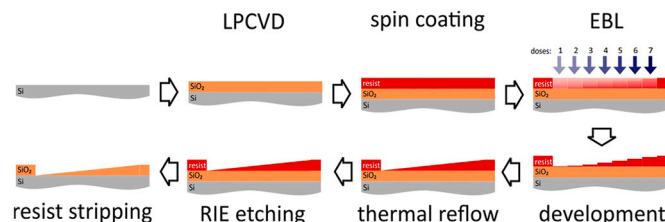


Fig. 2. Schematic of the fabrication steps of the 3D structured sensor surface.

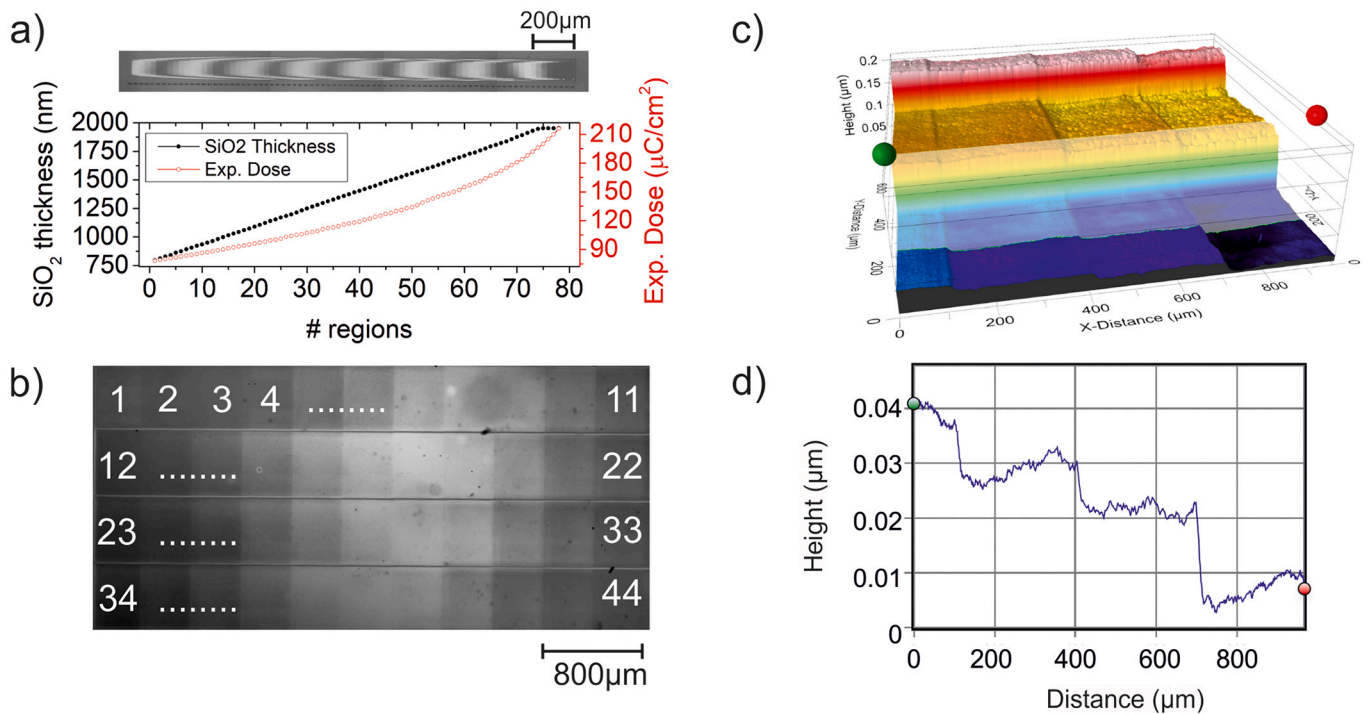


Fig. 3. (a) Top - microscope image of the first design of the structure; Bottom - SiO₂ thickness and EBL exposure dose of the structure versus index of regions, (b) Microscope image of the final 3D structure with 44 regions of linearly varying SiO₂ thickness in water illuminated with 458 ± 10 nm light, (c) Optical profilometer image of the structure in a region inside the sensor area shown in (b) obtained using a $\times 20$ objective lens, the area index changes sequentially along the small steps, while three of the four rows of the sensor can be distinguished. (d) Step height along the line shown in (c).

microscope using a $\times 4$ objective lens, a halogen light source with a 458 ± 10 nm bandpass filter (that can be easily fitted on any microscope), and a CMOS photodetector (Hamamatsu ORCA-Flash4.0 V3 CMOS detector) for the imaging. The thickness difference of two adjacent regions (around 15 nm) in water results in approximately 1% difference in reflectivity at 458 nm, which provides enough visual contrast and can be clearly distinguished from the microscope image of b. As illustrated in Fig. 3b) we used an index $i(1-44)$ to identify regions with different SiO₂ thickness values: $d_i \approx 1000(\text{nm}) + 15(\text{nm}) \times i$.

2.1. Biofunctionalization of the sensor's surface

The 3D structured chips, were first cleaned with acetone and 2-propanol, and then hydrophilized and further cleaned by immersion in a Piranha solution (1:1 H₂SO₄/H₂O₂, 30% v/v) for 20 min. After washing with distilled water and drying with N₂, the chips were immersed in a 2% (v/v) aqueous (3-aminopropyl)triethoxysilane (APTES) solution for 20 min. Finally, they were washed again with distilled water and dried with N₂ and then thermally cured for 20 min at 120 °C. The APTES-functionalized chips were left for at least 48 h at room temperature prior to spotting with a 50 μg/mL AFB₁-bovine serum albumin conjugate solution (AFB₁-BSA; Aokin AG, Germany) in 0.05 M carbonate buffer, pH 9.2, using the BioOdyssey Calligrapher Mini Arrayer (Bio-Rad Laboratories, Inc.). During spotting, the humidity was set at 75% and the temperature at 15 °C to avoid drying of the deposited solution, whereas after spotting the chips were washed with 10 mM Tris-HCl, pH 8.25, containing 9 g/L NaCl, and blocked through immersion for 1 h in 10 mg/mL BSA solution in 0.1 M NaHCO₃, pH 8.5. Following that, the surfaces were washed with distilled water, dried under N₂ flow and used for the assay.

2.2. Determination of AFB₁

Each biofunctionalized chip was assembled with a microfluidic cell,

placed on the docking station and equilibrated with assay buffer (50 mM Tris-HCl, pH 7.8, 9 g/L NaCl, 5 g/L BSA, 0.5 g/L NaN₃) for 3 min, prior to running 1:1 (v/v) mixtures of AFB₁ calibrators with a 1 μg/mL of anti-AFB₁ antibody (Aokin AG, Germany) solution in assay buffer for 7 min at a flow rate of 40 μL/min. Following that, a 10 μg/mL goat anti-mouse IgG antibody solution in assay buffer was flowed for 5 min. Finally, the biochip was washed 2 min with assay buffer and regenerated by passing 0.5% (w/v) SDS solution, adjusted at pH 1.3 with 0.1 M HCl, for 3 min, and then equilibrated again with assay buffer. In all steps, the solutions were run at a flow rate of 40 μL/min. Prior to the next measurement, the chip was equilibrated with assay buffer.

The reflectivity of the surface is expected to change due to the formation of the biomolecular adlayer, which is typically of the order of 1 nm. The signal of the CMOS pixel p , $I(p, a(t), \lambda)$ depends on the local thickness of the SiO₂ layer imaged, the adlayer thickness $a(t)$ which varies during the measurement, and the wavelength λ . The presence of an adlayer with varying thickness can be detected from the change in the reflected intensity recorder by the CMOS during the measurement:

$$\Delta I(p, a(t), \lambda) = I(p, a(t), \lambda) - I(p, a(0), \lambda) \quad (1)$$

where $a(0)$ is the adlayer thickness in the beginning of the measurement. From the images obtained we assign an average intensity in each rectangular region, which includes N_i pixels, as shown in Fig. 4(a-c):

$$\bar{\Delta I}_i = \frac{1}{N_i} \sum_{p \in i} \Delta I(p, a(t), \lambda) \quad (2)$$

to compensate for contrast variations due to bubbling or other image artifacts due to the flow during the experiment.

The progress of the assay was monitored by acquiring images of the sensor surface every 10 s. In particular, In Fig. 4(a-c), we present the difference ΔI for images taken at 3 different times along the assay ($t_1 = 10$ s, $t_2 = 900$ s and $t_3 = 1160$ s), where t_1 corresponds to the very beginning of the assay when the assay buffer was run over the surface, t_2

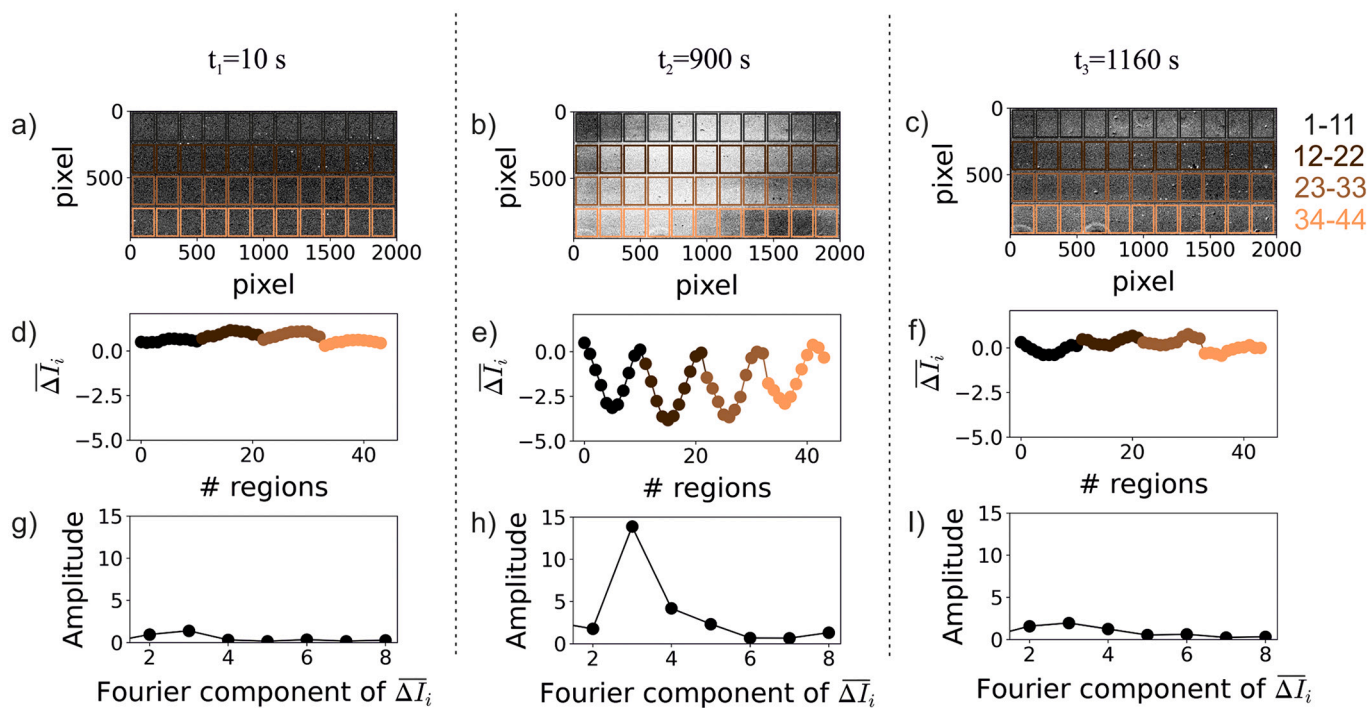


Fig. 4. (a-c) Image subtraction $\Delta I(p, a(t), \lambda = 458\text{nm})$, (d-f) Averaged intensity difference in each region $\overline{\Delta I}_i$ (Eq. 2), and (g-i) Fourier component of $\overline{\Delta I}_i$ for 3 different times t_1, t_2, t_3 where t_1 : at the initial equilibration with assay buffer, t_2 : during the 5-min reaction with the secondary antibody, and t_3 : during the regeneration step.

corresponds to reaction with the secondary antibody solution, and t_3 corresponds to the end of the assay when the surface was regenerated to remove all bound antibodies. When the adlayer thickness increases we clearly observe a sinusoidal variation of $\overline{\Delta I}_i$ with the thickness of the SiO_2 . For $t_2 = 900$ s (Fig. 4e) at least 4 periods can be clearly distinguished so that the variation of the reflectivity due to the adlayer which allows for an accurate determination of the amplitude of the variation by calculating the Fourier transform of $\overline{\Delta I}_i$ versus SiO_2 thickness, which is expected to be proportional to the thickness of the adlayer. As shown in

Fig. 4 h, the magnitude of the dominant Fourier component correlates directly and quantifies the adlayer thickness, where low image contrast ($t_1 = 10$ s and $t_3 = 1160$ s) suggests low adlayer thickness, while when the contrast is high ($t_2 = 900$ s) the adlayer thickness increases.

This procedure allows to monitor the progress of the assay as shown in Fig. 5, where the evolution of the dominant Fourier component upon running a zero AFB₁ calibrator solution is illustrated. Specifically, the signal recorded during step A where the chip is equilibrated with assay buffer does not detect any difference attributed to the formation of

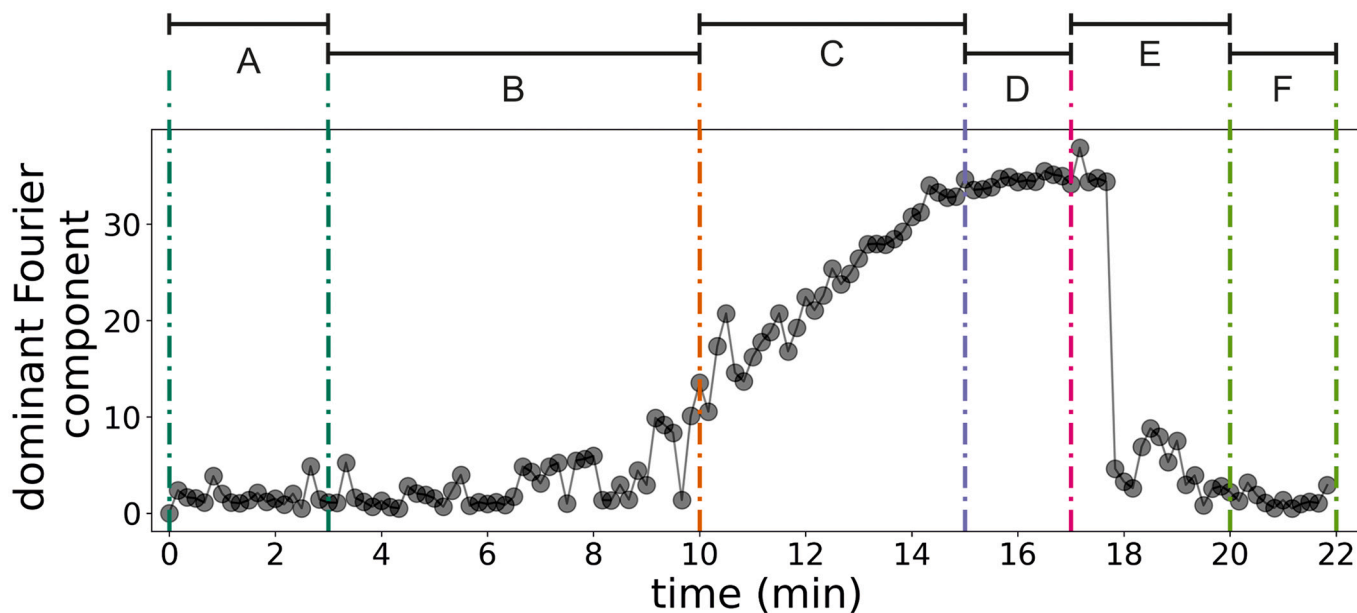


Fig. 5. (a) Real-time sensor response to AFB₁ calibrations prepared in assay buffer by monitoring the evolution of the dominant Fourier component. The sequence of solutions is: A – 3 min assay buffer, B – 7 min mixture of zero calibrator with the anti-AFB₁ antibody, C – 5 min goat anti-mouse IgG antibody, D – 2 min assay buffer, E – 3 min regeneration buffer, and F – 2 min assay buffer.

biomolecular adlayer as expected, while at step B, where the reaction of the specific anti-AFB₁ antibody with the immobilized onto the chip AFB₁-protein conjugate takes place, a change can be sensed at $t = 6.5$ min, 2 min after the start of introducing the anti-AFB₁ antibody on the 3D structured surface. The binding of the specific anti-AFB₁ antibody (primary antibody) can be detected up to the time the secondary antibody is introduced at step C (from 10 to 15 min), with a signal fluctuation at 8–9 min, which is attributed to the very small thickness (around 0.2 nm [19]) of the effective biomolecular layer corresponding to step B. The reaction with the secondary antibody, at step C, resulted in significant signal enhancement due to the binding of multiple secondary antibodies per molecule of surface bound specific antibody, while the signal is stable when assay buffer was run again over the chip at step D. Introduction of regeneration solution caused an abrupt decrease of the signal due to removal of bound primary and secondary antibody (step E) and equilibration with assay buffer stabilized the signal at a value close to the signal prior to assay (step F).

The signal obtained for the zero AFB₁ calibrator, depicted in Fig. 5, is the maximum signal obtained for this assay since a competitive immunoassay format is followed. In this assay format, detection sensitivity depends on the specific antibody binding affinity and the variation of the signal corresponding to zero calibrator. Thus, although a full calibration curve was not received, based on the performance of the same antibody in the WLRs sensor [17] and the similar variation of values received for repetitive measurements of the zero calibrator with the two sensors (<3.5%), it is expected that the assay detection limit would be lower than 0.1 ng/mL. Regarding the specificity of the detection based on previous studies with the same antibody [17, 20], it is anticipated that not significant cross-reactivity against AFB₂ or the major mycotoxins of the fumonisins and trichothecenes group are expected.

3. Conclusions

In this work we presented an alternative approach of the WLRs methodology for label-free detection of bioreactions. The proposed approach relies on a simple and cost-effective set-up in contrast with other optical label-free detection techniques, since the illumination does not require broadband light source but is based on LEDs or spectral filters, the signal is recorded by a camera and not a spectrometer and the fabrication of the biochips can be performed by cost-effective high-volume manufacturing employing UV or nanoimprint lithography instead of EBL. The first, proof-of-concept results on the detection of aflatoxin B1 are in a good agreement with similar study using the WLRs methodology [19] supporting the potential impact of the novel detection principle in application fields such as the food industry, the pharmaceutical industry and the bio diagnostics where on-site determinations are of utmost importance. Future work should focus on further optimization and evaluation of the proposed method for AFB₁ determination in food substrates and demonstration of the methodology for the detection of other analytes. In addition, an investigation of the minimum number of thickness-varying-regions and the optimal size of each region required should be carried out to further optimize the overall size of the sensing area. Lastly the simultaneous detection of multiple analytes should also be possible by increasing the size of the 3D structured chip to contain multiple sensing areas where each one will be functionalized with a different binding moiety for the binding of different biomolecules and signal from all areas will be obtained and processed simultaneously.

Funding

This research is co-financed by Greece and the European Union (European Social Fund—ESF) through the Operational Program “Human Resources Development, Education and Lifelong Learning 2014–2020” in the context of the project “HERON - Interferometric system based on a 3D structured biochip: an application to quantitative

determination of hazardous substances in food” (MIS 5047824).

Declaration of Competing Interest

None.

Acknowledgements

The authors are thankful to K. Toulouki for optical profilometer characterization of the 3D structured chips.

References

- [1] G. Zanchetta, R. Lanfranco, F. Giavazzi, T. Bellini, M. Buscaglia, Emerging applications of label-free optical biosensors, *Nanophotonics*. 6 (2017) 627–645, <https://doi.org/10.1515/nanoph-2016-0158>.
- [2] E. Gorodkiewicz, Z. Lukaszewski, Recent Progress in surface Plasmon resonance biosensors (2016 to Mid-2018), *Biosensors*. 8 (2018) 132, <https://doi.org/10.3390/bios8040132>.
- [3] S. Sang, Y. Zhang, Y. Zhao, Review on the design art of biosensors, *State Art Biosens. - Gen. Asp.* (2013), <https://doi.org/10.5772/52257>.
- [4] G. Gauglitz, A. Brecht, G. Kraus, W. Mahm, Chemical and biochemical sensors based on interferometry at thin (multi-) layers, *Sensors Actuators B Chem.* 11 (1993) 21–27, [https://doi.org/10.1016/0925-4005\(93\)85234-2](https://doi.org/10.1016/0925-4005(93)85234-2).
- [5] Y. Kurihara, T. Sawazumi, T. Takeuchi, Exploration of interactions between membrane proteins embedded in supported lipid bilayers and their antibodies by reflectometric interference spectroscopy-based sensing, *Analyst*. 139 (2014) 6016–6021, <https://doi.org/10.1039/C4AN00925H>.
- [6] A.K. Krieg, G. Gauglitz, Ultrasensitive label-free immunoassay for optical determination of amitriptyline and related tricyclic antidepressants in human serum, *Anal. Chem.* 87 (2015) 8845–8850, <https://doi.org/10.1021/acs.analchem.5b01895>.
- [7] Y. Zhang, Z. Wu, K. Li, X. Li, A. Yang, P. Tong, H. Chen, Allergenicity assessment on thermally processed peanut influenced by extraction and assessment methods, *Food Chem.* 281 (2019) 130–139, <https://doi.org/10.1016/j.foodchem.2018.12.070>.
- [8] D.L. Brandon, L.M. Adams, Milk matrix effects on antibody binding analyzed by enzyme-linked immunosorbent assay and Bi-layer Interferometry, *J. Agric. Food Chem.* 63 (2015) 3593–3598, <https://doi.org/10.1021/acs.jafc.5b01136>.
- [9] Konica Minolta RfS, Konica Minolta RfS. https://www.konicaminolta.jp/opt/support/catalog_download/rifs/pdf/rifs_catalog-en.pdf, 2010.
- [10] 2022. <https://www.sartorius.com/en/applications/life-science-research/label-free-detection/bli-technology>. (Accessed 26 February 2022).
- [11] M. Zavali, P.S. Petrou, S.E. Kakabakos, M. Kitsara, I. Raptis, K. Beltsios, K. Misiakos, Label-free kinetic study of biomolecular interactions by white light reflectance spectroscopy, *Micro Nano Lett.* 1 (2006) 94, <https://doi.org/10.1049/mnl:20065019>.
- [12] G. Koukouvinos, P. Petrou, K. Misiakos, D. Drygiannakis, I. Raptis, G. Stefanitis, S. Martini, D. Nikita, D. Goustouridis, I. Moser, G. Jobst, S. Kakabakos, Simultaneous determination of CRP and D-dimer in human blood plasma samples with white light reflectance spectroscopy, *Biosens. Bioelectron.* 84 (2016) 89–96, <https://doi.org/10.1016/j.bios.2015.11.094>.
- [13] G. Koukouvinos, D. Goustouridis, K. Karasiakos, S. Kakabakos, I. Raptis, P. Petrou, Rapid C-reactive protein determination in whole blood with a white light reflectance spectroscopy label-free immunosensor for point-of-care applications, *Sensors Actuators B Chem.* 260 (2018) 282–288, <https://doi.org/10.1016/j.snb.2018.01.008>.
- [14] G. Koukouvinos, Z. Tsiaila, P.S. Petrou, K. Misiakos, D. Goustouridis, A. Ucles Moreno, A.R. Fernandez-Alba, I. Raptis, S.E. Kakabakos, Fast simultaneous detection of three pesticides by a white light reflectance spectroscopy sensing platform, *Sensors Actuators B Chem.* 238 (2017) 1214–1223, <https://doi.org/10.1016/j.snb.2016.09.035>.
- [15] E. Stavra, P.S. Petrou, G. Koukouvinos, C. Kiritsis, I. Pirmettis, M. Papadopoulos, D. Goustouridis, A. Economou, K. Misiakos, I. Raptis, S.E. Kakabakos, Simultaneous determination of paraquat and atrazine in water samples with a white light reflectance spectroscopy biosensor, *J. Hazard. Mater.* 359 (2018) 67–75, <https://doi.org/10.1016/j.jhazmat.2018.07.029>.
- [16] G. Koukouvinos, A. Metheniti, C.-E. Karachaliou, D. Goustouridis, E. Livanou, K. Misiakos, I. Raptis, A. Kondili, P. Miniati, P. Petrou, S. Kakabakos, White light reflectance spectroscopy biosensing system for fast quantitative prostate specific antigen determination in forensic samples, *Talanta*. 175 (2017) 443–450, <https://doi.org/10.1016/j.talanta.2017.07.074>.
- [17] V. Anastasiadis, G. Koukouvinos, P.S. Petrou, A. Economou, J. Dekker, M. Harjanne, P. Heimala, D. Goustouridis, I. Raptis, S.E. Kakabakos, Multiplexed mycotoxins determination employing white light reflectance spectroscopy and

- silicon chips with silicon oxide areas of different thickness, *Biosens. Bioelectron.* 153 (2020), 112035, <https://doi.org/10.1016/j.bios.2020.112035>.
- [18] T. Mpatzaka, G. Papageorgiou, N. Papanikolaou, E. Valamontes, T. Ganetsos, D. Goustouridis, I. Raptis, G. Zisis, In-situ characterization of the development step of high-resolution e-beam resists, *Micro Nano Eng.* 9 (2020), 100070, <https://doi.org/10.1016/j.mne.2020.100070>.
- [19] D. Tsounidi, G. Koukouvinos, P. Petrou, K. Misiakos, G. Zisis, D. Goustouridis, I. Raptis, S.E. Kakabakos, Rapid and sensitive label-free determination of aflatoxin M1 levels in milk through a white light reflectance spectroscopy immunosensor, *Sensors Actuators B Chem.* 282 (2019) 104–111, <https://doi.org/10.1016/j.snb.2018.11.026>.